ADVANCED FUNCTIONAL MATERIALS
www.afm-journal.de

Tuning Local Molecular Orientation–Composition Correlations in Binary Organic Thin Films by Solution Shearing

Wei Ma, Julia Reinspach, Yan Zhou, Ying Diao, Terry McAfee, Stefan C. B. Mannsfeld, Zhenan Bao, and Harald Ade**

A general impact of solution shearing on molecular orientation correlation is observed in polymer:fullerene organic solar cells in which one of the components forms fibrils or aggregates. Further investigation with polarized soft X-ray scattering reveals that solution shearing induces more face-to-face orientation relative to the interface of two components compared to spin-coating. This impact is shearing speed dependent, that is, slow shearing speed can induce more face-to-face orientation than a fast shearing speed. These results demonstrate that solution shearing is an effective method to control the relative molecular orientation. Solution shearing can also modify the domain size and average composition variations.

1. Introduction

Spin-coating,[1] zone casting,[2] dip-coating,[3] roll-to-roll printing,[4] slot die coating,[5] spray painting,[6] and solution shearing[7–9] are widely used technologies to create multifunctional thin polymer films from solutions. These tools have been extensively applied to fabricate a number of products in both industrial and academic fields, such as food packing, bioelectrodes, electrical sensor, and CO_2 detectors.[7,9–12] They are also promising technologies to fabricate low-cost, large-area, and flexible organic electronics.[13–17] Beyond intrinsic performance, large-area and fast fabrication are considered to be crucial to achieve commercially feasible wide-scale production of any thin film technologies. Among the fabrication tools mentioned, the solution shearing coating method is particularly advantageous to meet these requirements. It not only allows the fast fabrication of organic thin films over a large area, but also shows great ability to manipulate the molecular packing and morphology on micro or even nanoscopic length scales in, for example, a single-component organic thin films transistor.[7,17] It is known that morphology and phase separation control are some of the most important aspects to achieve high performance organic devices for both single and double components systems.[18–20] Similar considerations apply to any multicomponent functional thin film. Therefore, it is critical to study the impact of the shear coating on manipulating the morphology, phase separation, or orientation correlations of two components organic thin films.

One of the most important two-component functional thin film application is organic solar cell (OSC) technology. It is known that the OSC morphology is critical for the performance. The ideal morphology of bulk heterojunction (BHJ) organic solar cell active layer consists of an interpenetrating network (≈10 nm lateral dimensions) of electron donor (D) and acceptor (A) materials, exhibiting a large interfacial area where photon generated excitons can split into holes and electrons that are subsequently transported to the electrodes.[16] Thus, suitable domain sizes at the length scale of the exciton diffusion length[21,22] and pure enough domains to reduce bimolecular recombination[23–25] have all been known to be critical factors that control the performance of OSC devices. As a more recent concept in the structure of organic solar cells, molecular orientation at and relative to the D/A interface has been shown to be also an important factor effecting the performance of solar cells.[24,26–33] Molecular orientation relative to donor/acceptor interfaces can be observed in complex BHJ morphologies by anisotropic scattering via polarized resonant soft X-ray scattering (R-SoXS) in polymer:polymer and polymer:fullerene devices.[24,30–34] A face-on orientation of the donor materials molecular backbone, with π orbital pointing to the acceptor [6,6]-Phenyl C_{61} butyric acid methyl ester (PCBM) phase, is considered to be the favorable configuration due to enhanced electronic overlapping.[28] Molecular orientation can even be the determining factor in some cases

Prof. W. Ma
State Key Laboratory for Mechanical Behavior of Materials
Xi'an Jiaotong University
Xi'an 710049, China
Prof. W. Ma, T. McAfee, Prof. H. Ade
Department of Physics
North Carolina State University
Raleigh, NC 27695, USA
E-mail: harald_ade@ncsu.edu
Dr. J. Reinspach, Dr. Y. Zhou, Dr. Y. Diao, Prof. Z. Bao
Department of Chemical Engineering
Stanford University
Stanford, CA 94305, USA
E-mail: zbao@stanford.edu
Dr. S. C. B. Mannsfeld[+]
Stanford Synchrotron Radiation Lightsource
SLAC National Accelerator Laboratory
Menlo Park, CA 94025, USA
[+]Present address: Center for Advancing Electronics Dresden, Dresden University of Technology, 01062 Dresden, Germany

DOI: 10.1002/adfm.201500468

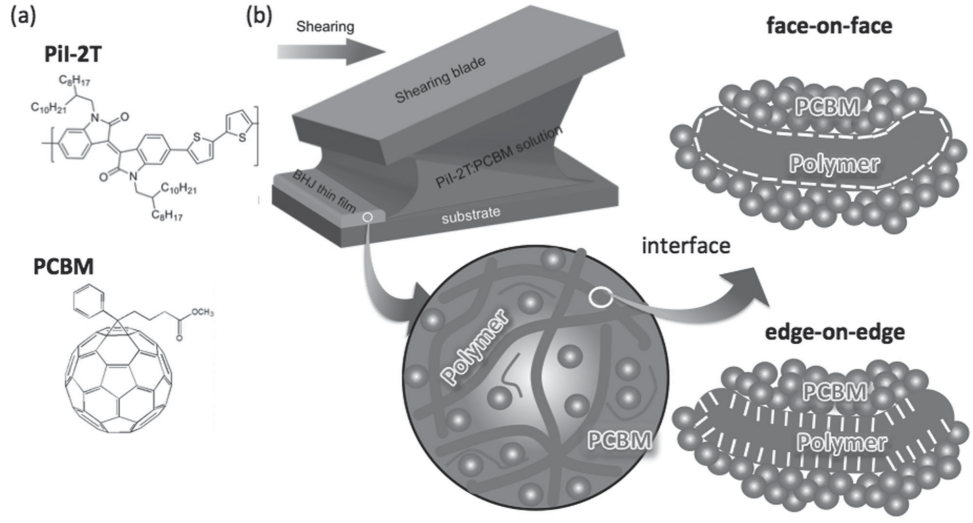

Scheme 1. a) Chemical structure of PCBM and PiI-2T and b) schematic illustration of the solution-shear coating and schematic for the face-on-face and edge-on-edge orientations. The white bars inside the polymer-rich phase represent the polymer backbone near the interface of polymer and fullerene.

with strong correlations to device performance, instead of other structural characteristics, such as domain size, domain purity, and polymer packing/crystallinity.[31] The observed molecular orientation is sensitive to the materials and processing solvent used.[24,30–32] It is in the context of ongoing studies on organic devices what we discovered that solution shearing could modify the degree molecular orientation correlations of the matrix polymer. We find that the lower solution-shearing speed utilized results in a higher molecular orientational order. Although this discovery should ultimately have ramifications for OSC devices, the correlation to the device performance is outside the scope of the current work due to complexities arising from thickness differences as a function of shearing speed and concurrent changes in performance related parameters that are currently difficult to disentangle. We observe anisotropic scattering and thus local molecular orientation correlations in two systems and propose that the shearing modifies fibrillar aggregation and its spatial arrangements. Due to their anisotropic nature, fibrils forming in the viscous solution should be sensitive to the shear produced by the coating method, and consequently, the local orientation correlations of all materials exhibiting anisotropic shapes or aggregates should be able to be manipulated with the solution shearing method.

In order to manipulate the local molecular orientation correlations by shear coating, we investigate PiI-2T:PCBM blends. The chemical structures of PiI-2T and PCBM are shown in **Scheme 1**a. The PiI-2T:PCBM blend ratio is 1:1.5 by weight. Most conjugated polymers have reported densities between 1.1 and 1.3 g cm^{-3}.[35,36] The reported density of PCBM is about 1.5 g cm^{-3}.[37] Thus, the estimated volume ratio is roughly 1:1.2 for our PiI-2T:PCBM blend. Spin-coating is the most widely used research fabrication method for organic electronics, and thus a spin-cast reference sample was prepared with the spin speed of 2000 rpm. Shearing speeds of 1 and 2.5 mm s^{-1} are examined. More processing details about solution shearing can be found in the Experimental Section.

2. Results and Discussion

To characterize the effect of the coating speed on phase separation of the polymer:fullerene blends, transmission R-SoXS is employed to probe the in-plane composition and orientation correlations and variations over length scales of ≈10–1000 nm.[22,34,38–42] A photon energy of 284.2 eV is selected to provide high polymer:fullerene contrast while avoiding high absorption at the absorption peaks (284.4 eV for fullerene), which generates C-1s core holes that can lead to beam damage[43] and fluorescence background. **Figure 1** shows the scattering profiles for the PiI-2T:PCBM blends with different processing conditions, i.e., spin-coating, and solution shearing at 1 and 2.5 mm s^{-1}. The scattering profiles represent the distribution function of the spatial frequencies, $s = q/2\pi$, of the composition correlations detected in the samples. The characteristic median length of the corresponding correlation distribution in real space is $\xi = 1/s_{median}$. We find that the spin-cast blend films have ξ of ≈60 nm. When the blend film is prepared by solution-shearing at 1 mm s^{-1}, ξ slightly increases to ≈100 nm. A higher

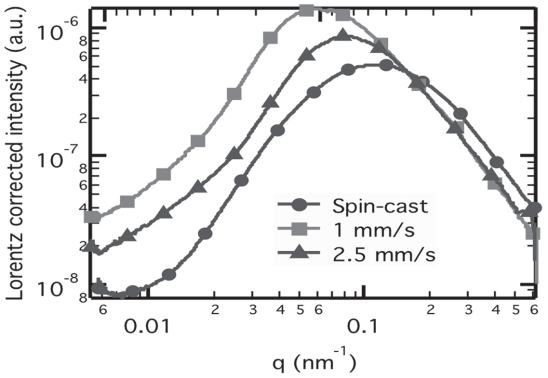

Figure 1. Azimuthally integrated R-SoXS profiles at 284.2 eV for the spin-cast blends, the sheared blends at 1 and 2.5 mm s^{-1}.

DOI: 10.1002/adfm.201500468

solution-shearing speed of 2.5 mm s^{-1} results in a ξ of ≈75 nm. These results are similar to the domain length scale revealed by atomic force microscopy (AFM) images (shown in Supporting Information, Figure S1). Importantly, a fibrillar structure with local orientation correlations is revealed on the surface of the blend, which will be discussed in detail for scattering anisotropy interpretation. Furthermore, the relative composition variation over the length scales probed (referred as relative average domain purity) in a two components blend can be revealed by calculating the Total Scattering Intensity (TSI) of the R-SoXS profiles.[44] Relative domain purities of 0.83, 1, and 0.87, for spin-casting and solution-shearing at 1 and 2.5 mm s^{-1}, are obtained, respectively. This suggests that sheared blends exhibit purer domains, on average, than spin-cast blends with 1 mm s^{-1} sheared blends having the purest domains. These results indicate that a slower solution-shearing speed resulted in considerably larger and purer domains, i.e., higher compositional variation in the blend.

To characterize the ability of solution shearing to manipulate the local molecular orientation correlations, the azimuthal variations in the R-SoXS 2D signal were analyzed.[34] The R-SoXS data of PiI-2T:PCBM solution sheared at 1 mm s^{-1} and randomly mounted relative to the electric field are shown in **Figure 2**b–d. The solution-shearing direction is marked with a thick arrow, and the perpendicular direction with a thin arrow. The topography of the sheared blend films revealed by AFM shows line patterns with a width of ≈10 µm and a height variation of ≈7 nm. The x-ray beam spot size is ≈100–200 µm, and the scattering thus integrates over multiple periods of this surface pattern. Figure 2b,c shows the R-SoXS scattering patterns with horizontally polarized x-rays at 284.2 and 285.2 eV, respectively. Note that the anisotropic scattering pattern is tilted, i.e., the most intense ***Z*** scattering sector is not perfectly aligned (parallel or perpendicular) with the electric field, which has not been reported before for two components blends.[24,30,34] We further note that the vector ***Z*** can be decomposed to the vector perpendicular to the solution-shearing direction (***S***⊥) and the vector perpendicular to the electric field of X-rays (***E***⊥). In addition, at 284.2 eV, where the scattering contrast between materials (PiI-2T:PCBM) dominates the R-SoXS scattering, ***Z***

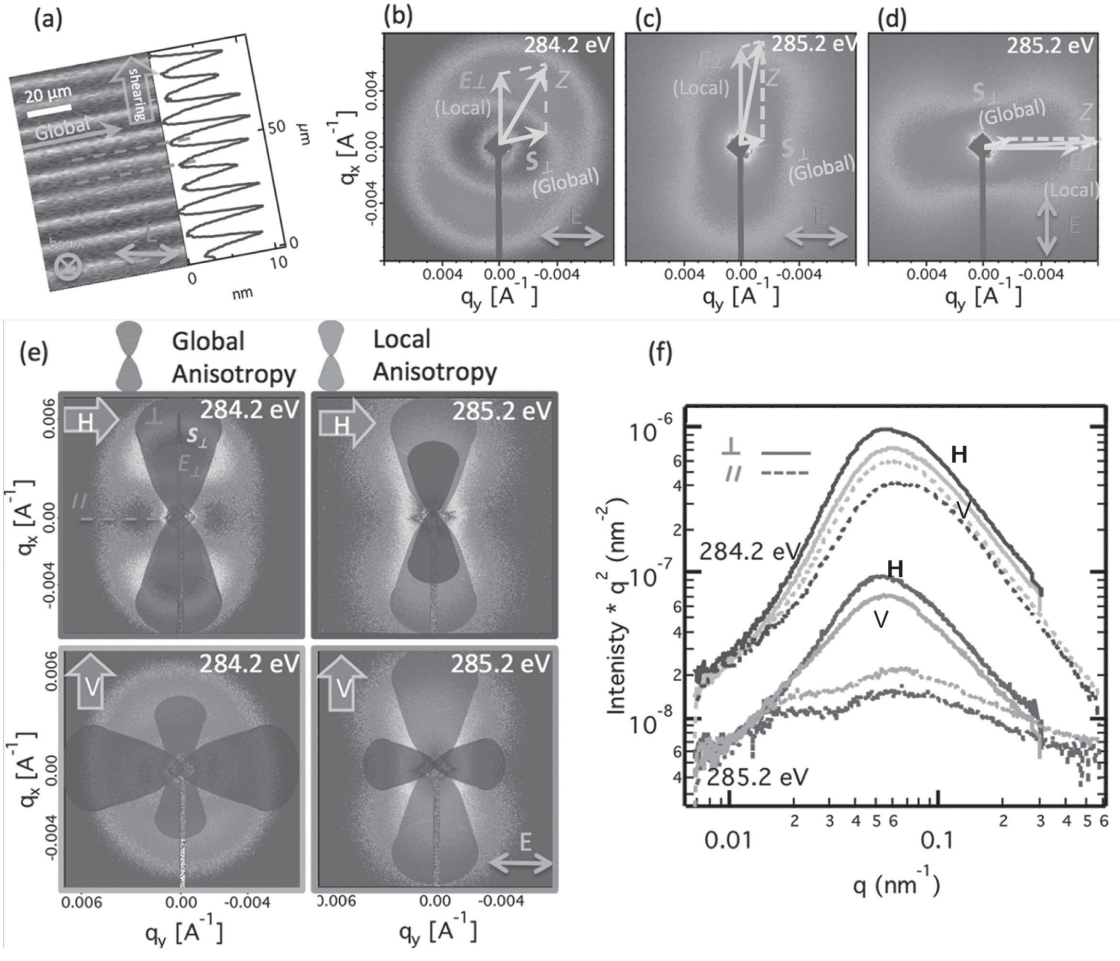

Figure 2. P-SoXS 2D scattering pattern of 1 mm s^{-1} sheared blend at different photon energies, and with different polarization and sample rotations. a) Atomic force microscopy of the blend films. The shearing direction is marked with the thick arrow, and the thin arrow presents the direction perpendicular to the shearing direction. 2D scattering pattern of the randomly loaded sample at b) 284.2 eV with horizontal polarization, c) 285.2 eV with horizontal polarization, d) 285.2 eV with vertical polarization, and e) 2D scattering pattern of sample aligned with the shearing direction horizontally and vertically at 284.2 and 285.2 eV with a horizontally polarized beam. f) Scattering profiles from Lorentz corrected sector averages of data in Figure 2e.

is closer to $S\perp$; and at 285.2 eV where the polymer orientation contrast (parallel aligned polymer:perpendicular aligned polymer) dominates the scattering, Z moves closer to $E\perp$. These findings strongly suggest that both materials contrast and orientation contrast impact the titled scattering anisotropy.[24]

Scattering anisotropy relative to the direction of the electric filed has been previously reported and delineated. Increased scattering perpendicular to the electric field at energies below 287 eV indicates a local face-to-face orientation correlation of the polymer in polymer:fullerene blends, while increased scattering parallel to the electric filed indicates an edge-to-edge correlation.[24,30–32,34] The detailed interpretation is illustrated in Supporting Information, Figure S2.[34] The origin of the scattering anisotropy is the same for the fibril-like structure discussed in the literature.[32] Hence, the observed $E\perp$ suggests a local face-on polymer backbone orientation configuration relative to the polymer:fullerene interface (as illustrated in Scheme 1b) for the fibril-like structure. The magnitude of the scattering anisotropy is proportional to the fraction of the molecules that are aligned. Consequently, $E\perp$ can be concluded to be associated with this local orientational anisotropy. The origin of $S\perp$ is not yet completely understood, but it is clearly related to the shearing and likely originates from the equivalent of an average asymmetric "volume fraction" along the two orthogonal directions as the domains are distorted by the shearing process. Due to the slightly higher acceptor amount, the blends have an average 1:1.2 volume fraction and given that the scattering intensity is proportional to $\psi(1-\psi)$ (where ψ is the volume fraction of one of the components), it is reasonable to surmise that the spin-coated blends show an overall asymmetric length fraction in the orthogonal directions defined by the shearing direction. The solution-shearing process potentially elongates the dispersed domains along the shearing direction (as shown in Supporting Information, Figure S3) and at the same time reduces the width of the dispersions along the direction perpendicular to the shearing direction. This would cause a more symmetric length fraction along the direction perpendicular to the shearing, which enhances X-ray scattering. Conversely, in the direction of shearing, the scattering is reduced to a now more unfavorable $\psi(1-\psi)$ product in that direction. Switching the polarization of x-rays from horizontal to vertical at 285.2 eV (Figure 2d) confirms this model. Since the locally probed molecular orientation rotates with the electric field while the global scattering is stationary, the Z direction is located between the unchanged $S\perp$ and the rotated $E\perp$ (compare to Figure 2c). Z rotates by more than 45° as the scattering due to local molecular orientation dominates at 285.2 eV. This confirms that both the local molecular orientation correlations and the asymmetric length fraction (a global asymmetry related to the shearing) contribute to the total scattering anisotropy observed by P-SoXS.

Taking advantage of the fact that local anisotropy and global anisotropy exhibit different sample rotation sensitivities, it is possible to differentiate between the two contributions. This is most easily done by aligning the sample with the shearing direction parallel (H) or perpendicular (V) to the electric field vector of the X-ray (referred to as horizontal and vertical sample directions). Figure 2e shows the R-SoXS results at 284.2 and 285.2 eV of 1 mm s^{-1} sheared blends for the two sample orientations. The corresponding sector profiles are displayed in Figure 2f. For the horizontally (H) orientated blend, the local molecular orientation related anisotropy ($E\perp$) and the shearing direction related anisotropy ($S\perp$) overlap in the vertical direction at 284.2 eV, which produces a significant enhancement in the total scattering anisotropy. When the sample is rotated to the vertical orientation, the scattering is more isotropic (also shown in Figure 2f) as $S\perp$ and $E\perp$ are orthogonally aligned and compensate the effects of each other. A similar observation is obtained when 285.2 eV X-rays are employed.

To analyze the local and global anisotropy more quantitatively, the total scattering anisotropy is defined as the difference of sector scattering intensity (SSI) perpendicular and parallel to the electric field direction over the sum (see Equation (1). Regarding the sample with the horizontal shearing direction (H), the local anisotropy and global anisotropy overlap in the vertical direction (shown Figure 2e) and the total scattering anisotropy is the sum of the two

$$\begin{aligned}\text{Anisotropy}^{H} &= \frac{\text{SSI}^{H}_{\text{perp.}} - \text{SSI}^{H}_{\text{parall.}}}{\text{SSI}^{H}_{\text{perp.}} + \text{SSI}^{H}_{\text{parall.}}} \\ &= \text{Anisotropy}^{Local} + \text{Anisotropy}^{Global}\end{aligned} \quad (1)$$

For the sample with the vertical shearing direction (V), local and global anisotropies are located in different directions (as shown in Figure 2e) and the total anisotropy is the difference between the two

$$\begin{aligned}\text{Anisotropy}^{V} &= \frac{\text{SSI}^{V}_{\text{perp.}} - \text{SSI}^{V}_{\text{parall.}}}{\text{SSI}^{V}_{\text{perp.}} + \text{SSI}^{V}_{\text{parall.}}} \\ &= \text{Anisotropy}^{\text{Local}} - \text{Anisotropy}^{\text{Global}}\end{aligned} \quad (2)$$

Thus, the local anisotropy is equal to

$$\text{Anisotropy}^{\text{Local}} = \frac{\text{Anisotropy}^{H} + \text{Anisotropy}^{V}}{2} \quad (3)$$

and the global anisotropy is equal to

$$\text{Anisotropy}^{\text{Global}} = \frac{\text{Anisotropy}^{H} - \text{Anisotropy}^{V}}{2} \quad (4)$$

Using these equations, the total scattering anisotropy, the anisotropy induced by local molecular orientation, and the anisotropy induced by global asymmetric volume fraction are calculated for the spin-cast, sheared at 1 and 2.5 mm s^{-1} blends, respectively, for the photon energy range of 280–287 eV. The results of the total scattering anisotropy are shown in **Figure 3**a. The spin-cast blend is globally isotropic (Supporting Information, Figure S4), and thus the total anisotropy only originates from the local molecular orientation relative to the interface. Its energy dependence can thus be used as an internal reference standard. In the blend sheared at 1 mm s^{-1}, the anisotropy is clearly enhanced when the sample is horizontally placed where

Adv. Funct. Mater. 2015,
DOI: 10.1002/adfm.201500468

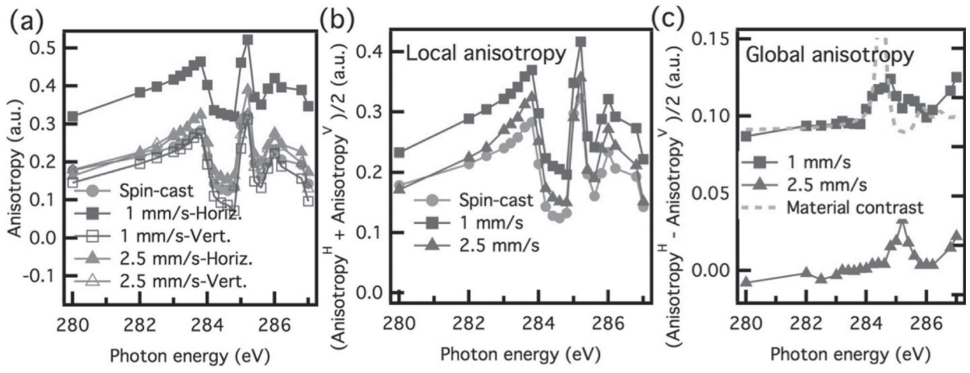

Figure 3. a) Thickness normalized scattering anisotropy of the spin-cast, sheared 1 and 2.5 mm s^{-1} blends with horizontal and vertical aligned sample rotation as a function of the photon energy, b) the calculated local anisotropy, and c) the calculated global anisotropy.

local and global anisotropies are overlapping. The anisotropy of the vertically placed blends is reduced due to the compensating effect discussed above. At a higher solution-shearing speed of 2.5 mm s^{-1}, horizontally and vertically placed films exhibit only slight differences, which indicates that the rotation of the sample has limited impact on the total anisotropy.

The energy dependences of the local anisotropy and global anisotropy are displayed in Figure 3b,c, respectively. The spin-cast blend shows the weakest local anisotropy and the blend sheared at 1 mm s^{-1} the highest. The substantial difference indicates that solution-shearing can significantly improve the molecular orientation correlations. Interestingly, the local anisotropy for the low solution-shearing speed 1 mm s^{-1} is larger than the high solution-shearing speed of 2.5 mm s^{-1}. This might result from shearing induced disorder, the film drying process, and the domain growth kinetics, which is the subject for further future investigations. This suggests that the solution-shearing speed is potentially a useful factor to manipulate the morphology and molecular orientation in materials that show aggregation in at least one component. Figure 3c plots the energy dependence of the global anisotropy and as mentioned above (Figure 3a), the 2.5 mm s^{-1} sheared blend exhibits weak global anisotropy. In contrast, the 1 mm s^{-1} sheared blend shows a strong global anisotropy. Furthermore, the energy dependence of the global anisotropy is very different from the energy dependences of the local anisotropy and follows approximately the materials contrast between PiI-2T and PCBM (Figure 3c). This confirms that the origin of the anisotropy associated with the shearing direction is related to an asymmetry in material composition distributions rather than molecular orientation correlations.

As a first step toward assessing the generality of our discovery, we processed and characterized poly(3-hexylthiophene) (P3HT):PCBM, by comparing spin-coating with solution shearing at 1 and 5 mm s^{-1}. Again, variations in scattering anisotropy related to differences in molecular orientation correlations could be observed. The results are displayed in Supporting Information, Figure S5. The scattering anisotropy observed is induced only by the local molecular orientations, i.e., without a global, shearing direction related component. We find that the scattering pattern of the 1 mm s^{-1} sheared blend is most anisotropy, and spin-cast blend and 5 mm s^{-1} sheared blends are more isotropic at 285.4 eV. Quantitative analysis using the same method as above reveals that the anisotropy for spin-cast, solution shearing at 1 and 5 mm s^{-1} are 0.055, 0.191, and 0.056, respectively. This system shows strong q-dependent anisotropy (energy-dependent R-SoXS of 1 mm s–1 shown in Supporting Information, Figure S6) and thus further optical modeling needs to be done to figure out the spatial orientation (face-on vs. edge-on). However, it is clearly shown that shearing affects the orientation of polymer blend films, which is similar to those observed for PiI-2T:PCBM. This strongly suggests that the manipulation of aggregate orientation correlations achievable with shear-coating is a new independent means of manipulations local molecular ordering.

3. Conclusion

In conclusion, we have discovered the impact of solution-coating conditions on the molecular orientation correlations in thin polymer:fullerene films in which one of the components (i.e., polymer) forms fibrils or aggregates whose orientations are locally correlated. We revealed that the slower solution-shear speed of the two speeds utilized enhanced the face-to-face molecular correlations of the polymer the most. The shearing also modifies the domain size and average composition variations. Our work indicates that manipulation of molecular orientation correlations and thus also the ordering relative to an interface of a two components system can be achieved by the solution-shearing coating methods. This opens up a new and exciting possibility for controlling aggregation in drying solutions under shear, and thus the morphology and phase separation including the interface structure. The method should be general and thus be of interest for any system in which at least one component aggregates. An immediate potential application might be the improvement of OSCs performance in systems that are difficult to control with spin-casting or other conventional methods.

4. Experimental Section

Materials: Synthesis of PiI-2T (M_n = 12.1 K g mol^{-1}, PDI = 2.98) was reported in the prior literature[45] and PCBM was purchased from Nano-C. The ultradry solvents DCB used in device fabrication process were purchased from Sigma-Aldrich.

Shear Coating:[46] The PII-2T:PCBM blend was prepared at 10 mg mL^{-1} concentration in DCB solution. As substrates, native oxide silicon wafers (25 mm × 12 mm, 25 mm in shearing direction) were used. They were first cleaned for 20 min by a UV-ozone treatment and then spin-coated with PSS (140 nm) (in H_2O). The substrates were then coated by solution shearing at a substrate temperature of T = 110 °C, a blade–substrate distance of 100 µm, and a blade–substrate angle of 1°. Samples were removed from the heated substrate stage and cooled down in air without additional control. Two shearing speeds were investigated, i.e., 1 and 2.5 mm s^{-1}. The solution shearing was performed under ambient conditions with temperature of 21 °C and typical humidity of 30–44%. After shearing, the samples were left on the heated substrate stage for 1 min to ensure evaporation of the solvent.

Measurements: The thickness of the active layer was controlled by changing the spin speed during the spin-coating process and by using different shearing speeds and measured with an AFM (MFP-3D, Asylum Research). R-SoXS transmission measurements were performed at beamline 11.0.1.2 at the Advanced Light Source (ALS).[47] Samples for R-SoXS measurements were first prepared on a PEDOT:PSS modified Si substrate as mentioned above, and then transferred to a 1 mm × 1 mm, 100-nm-thick Si3N4 membrane supported by a 5 mm × 5 mm, 200-µm-thick Si frame (Norcada Inc.). 2D scattering patterns were collected on an in-vacuum CCD camera (Princeton Instrument PI-MTE).

Supporting Information

Supporting Information is available from the Wiley Online Library or from the author.

Acknowledgements

X-ray characterization and analysis by NCSU was supported by the US Department of Energy, Office of Science, Basic Energy Science, Division of Materials Science and Engineering, under Contract No. DE-FG02-98ER45737. X-ray data were acquired at beamlines 11.0.1.2 at the Advanced Light Source, which is supported by the Director, Office of Science, Office of Basic Energy Sciences of the US Department of Energy under Contract No. DE-AC02-05CH11231. S.C.B.M., Z.B., and Y.D. acknowledge support by the Department of Energy, Bridging Research Interactions through the collaborative Development Grants in Energy (BRIDGE) program under Contract No. DE-FOA-0000654-1588. Y. Z. and Z. B. acknowledge support from the Office of Naval Research (N00014-14-1-0142) for synthesis.

Received: February 4, 2015
Revised: February 26, 2015
Published online:

[1] Y. Liu, X. Wan, F. Wang, J. Zhou, G. Long, J. Tian, J. You, Y. Yang, Y. Chen, *Adv. Energy Mater.* **2011**, *1*, 771.
[2] M. J. Lee, D. Gupta, N. Zhao, M. Heeney, I. McCulloch, H. Sirringhaus, *Adv. Funct. Mater.* **2011**, *21*, 932.
[3] C. W. Sele, B. K. C. Kjellander, B. Niesen, M. J. Thornton, J. B. P. H. van der Putten, K. Myny, H. J. Wondergem, A. Moser, R. Resel, A. J. J. M. van Breemen, N. van Aerle, P. Heremans, J. E. Anthony, G. H. Gelinck, *Adv. Mater.* **2009**, *21*, 4926.
[4] R. R. Søndergaard, M. Hösel, F. C. Krebs, *J. Polym. Sci. Polym. Phys. Part B* **2013**, *51*, 16.
[5] L. Wengeler, B. Schmidt-Hansberg, K. Peters, P. Scharfer, W. Schabel, *Chem. Eng. Process.* **2011**, *50*, 478.
[6] K. Fujita, T. Ishikawa, T. Tsutsui, *Jpn. J. Appl. Phys.* **2002**, *41*, L70.
[7] Y. Diao, B. C. Tee, G. Giri, J. Xu, D. H. Kim, H. A. Becerril, R. M. Stoltenberg, T. H. Lee, G. Xue, S. C. B. Mannsfeld, Z. Bao, *Nat. Mater.* **2013**, *12*, 665.
[8] H. Becerril, M. Roberts, Z. Liu, J. Locklin, Z. Bao, *Adv. Mater.* **2008**, *20*, 2588.
[9] G. Giri, S. Park, M. Vosgueritchian, M. M. Shulaker, Z. Bao, *Adv. Mater.* **2014**, *26*, 487.
[10] Q. Meng, F. Zhang, Y. Zang, D. Huang, Y. Zou, J. Liu, *J. Mater. Chem. C* **2014**, *2*, 1264.
[11] S. Baek, R. Green, A. Granville, P. Martens, L. Poole-Warren, *J. Mater. Chem. C* **2013**, *1*, 3803.
[12] G. Telipan, in *2nd Electron. Syst. Technol. Conf.*, **2008**, pp. 1231–1234.
[13] H. Klauk, U. Zschieschang, J. Pflaum, M. Halik, *Nature* **2007**, *445*, 745.
[14] B. Crone, A. Dodabalapur, Y. Lin, R. Filas, Z. Bao, A. LaDuca, R. Sarpeshkar, H. Katz, W. Li, *Nature* **2000**, *403*, 521.
[15] G. H. Gelinck, H. E. A. Huitema, E. van Veenendaal, E. Cantatore, L. Schrijnemakers, J. B. P. H. van der Putten, T. C. T. Geuns, M. Beenhakkers, J. B. Giesbers, B.-H. Huisman, E. J. Meijer, E. M. Benito, F. J. Touwslager, A. W. Marsman, B. J. E. van Rens, D. M. de Leeuw, *Nat. Mater.* **2004**, *3*, 106.
[16] G. Li, R. Zhu, Y. Yang, *Nat. Photonics* **2012**, *6*, 153.
[17] R. Søndergaard, M. Hösel, D. Angmo, T. T. Larsen-Olsen, F. C. Krebs, *Mater. Today* **2012**, *15*, 36.
[18] M. A. Ruderer, P. Muller-Buschbaum, *Soft Matter* **2011**, *7*, 5482.
[19] Y.-J. Cheng, S.-H. Yang, C.-S. Hsu, *Chem. Rev.* **2009**, *109*, 5868.
[20] B. C. Thompson, J. M. J. Fréchet, *Angew. Chem. Int. Ed.* **2008**, *47*, 58.
[21] J. Peet, J. Y. Kim, N. E. Coates, W. L. Ma, D. Moses, A. J. Heeger, G. C. Bazan, *Nat. Mater.* **2007**, *6*, 497.
[22] L. Ye, S. Zhang, W. Ma, B. Fan, X. Guo, Y. Huang, H. Ade, J. Hou, *Adv. Mater.* **2012**, *24*, 6335.
[23] A. Stuart, J. R. Tumbleston, H. Zhou, H. Ade, W. Li, W. You, *J. Am. Chem. Soc.* **2013**, *135*, 1806.
[24] W. Ma, J. Tumbleston, M. Wang, E. Gann, F. Huang, H. Ade, *Adv. Energy Mater.* **2013**, *3*, 864.
[25] S. Albrecht, S. Janietz, W. Schindler, J. Frisch, J. Kurpiers, J. Kniepert, S. Inal, P. Pingel, K. Fostiropoulos, N. Koch, D. Neher, *J. Am. Chem. Soc.* **2012**, *134*, 14932.
[26] S. Verlaak, D. Beljonne, D. Cheyns, C. Rolin, M. Linares, F. Castet, J. Cornil, P. Heremans, *Adv. Funct. Mater.* **2009**, *19*, 3809.
[27] J. D. Zimmerman, X. Xiao, C. K. Renshaw, S. Wang, V. V Diev, M. E. Thompson, S. R. Forrest, *Nano Lett.* **2012**, *12*, 4366.
[28] B. P. Rand, D. Cheyns, K. Vasseur, N. C. Giebink, S. Mothy, Y. Yi, V. Coropceanu, D. Beljonne, J. Cornil, J.-L. Brédas, J. Genoe, *Adv. Funct. Mater.* **2012**, *22*, 2987.
[29] A. Ojala, A. Petersen, A. Fuchs, R. Lovrincic, C. Pölking, J. Trollmann, J. Hwang, C. Lennartz, H. Reichelt, H. W. Höffken, A. Pucci, P. Erk, T. Kirchartz, F. Würthner, *Adv. Funct. Mater.* **2012**, *22*, 86.
[30] W. Ma, L. Ye, S. Zhang, J. Hou, H. Ade, *J. Mater. Chem. C* **2013**, *1*, 5023.
[31] J. R. Tumbleston, L. Yang, B. A. Collins, A. C. Stuart, E. Gann, W. Ma, W. You, H. Ade, *Nat. Photonics* **2014**, *8*, 385.
[32] F. Liu, C. Wang, J. K. Baral, L. Zhang, J. J. Watkins, A. L. Briseno, T. P. Russell, *J. Am. Chem. Soc.* **2013**, *135*, 19248.
[33] C. R. McNeill, H. Ade, *J. Mater. Chem. C* **2013**, *1*, 187.
[34] B. A. Collins, J. E. Cochran, H. Yan, E. Gann, C. Hub, R. Fink, C. Wang, T. Schuettfort, C. R. McNeill, M. L. Chabinyc, H. Ade, *Nat. Mater.* **2012**, *11*, 536.
[35] M. Reyes-Reyes, R. López-Sandoval, J. Arenas-Alatorre, R. Garibay-Alonso, D. L. Carroll, A. Lastras-Martinez, *Thin Solid Films* **2007**, *516*, 52.
[36] O. V. Mikhnenko, H. Azimi, M. Scharber, M. Morana, P. W. M. Blom, M. A. Loi, *Energy Environ. Sci.* **2012**, *5*, 6960.

[37] P. H. Wöbkenberg, D. D. C. Bradley, D. Kronholm, J. C. Hummelen, D. M. de Leeuw, M. Cölle, T. D. Anthopoulos, *Synth. Met.* **2008**, *158*, 468.
[38] W. Chen, T. Xu, F. He, W. Wang, C. Wang, J. Strzalka, Y. Liu, J. Wen, D. J. Miller, J. Chen, K. Hong, L. Yu, S. B. Darling, *Nano Lett.* **2011**, *11*, 3707.
[39] B. A. Collins, H. Ade, *J. Electron Spectrosc. Relat. Phenom.* **2012**, *185*, 119.
[40] S. Swaraj, C. Wang, H. Yan, B. Watts, J. Lüning, C. R. McNeill, H. Ade, *Nano Lett.* **2010**, *10*, 2863.
[41] H. Yan, B. A. Collins, E. Gann, C. Wang, H. Ade, *ACS Nano* **2012**, *6*, 677.
[42] C. Guo, Y. Lin, M. D. Witman, K. A. Smith, C. Wang, A. Hexemer, J. Strzalka, E. D. Gomez, R. Verduzco, *Nano Lett.* **2013**, *13*, 2957.
[43] T. Coffey, S. G. Urquhart, H. Ade, *J. Electron Spectrosc. Relat. Phenom.* **2002**, *122*, 65.
[44] B. A. Collins, Z. Li, J. R. Tumbleston, E. Gann, C. R. McNeill, H. Ade, *Adv. Energy Mater.* **2013**, *3*, 65.
[45] L. Fang, Y. Zhou, Y.-X. Yao, Y. Diao, W.-Y. Lee, A. L. Appleton, R. Allen, J. Reinspach, S. C. B. Mannsfeld, Z. Bao, *Chem. Mater.* **2013**, *25*, 4874.
[46] H. Becerril, M. Roberts, Z. Liu, J. Locklin, Z. Bao, *Adv. Mater.* **2008**, *20*, 2588.
[47] E. Gann, A. T. Young, B. A. Collins, H. Yan, J. Nasiatka, H. A. Padmore, H. Ade, A. Hexemer, C. Wang, *Rev. Sci. Instrum.* **2012**, *83*, 045110.